

Strong Pairing Originated from an Emergent \mathbb{Z}_2 Berry Phase in $\text{La}_3\text{Ni}_2\text{O}_7$

Jia-Xin Zhang,^{1,*} Hao-Kai Zhang,^{1,†} Yi-Zhuang You,² and Zheng-Yu Weng¹

¹*Institute for Advanced Study, Tsinghua University, Beijing 100084, China*

²*Department of Physics, University of California, San Diego, CA 92093, USA*

(Dated: August 12, 2024)

The recent discovery of high-temperature superconductivity in $\text{La}_3\text{Ni}_2\text{O}_7$ offers a fresh platform for exploring unconventional pairing mechanisms. Starting with the basic argument that the electrons in d_{z^2} orbitals nearly form local moments, we examine the effect of the Hubbard interaction U on the binding strength of Cooper pairs based on a single-orbital bilayer model with intralayer hopping t_{\parallel} and interlayer super-exchange J_{\perp} . By extensive density matrix renormalization group calculations, we observe a remarkable enhancement in binding energy as much as 10-20 times larger with U/t_{\parallel} increasing from 0 to 12 at $J_{\perp}/t_{\parallel} \sim 1$. We demonstrate that such a substantial enhancement stems from a kinetic-energy-driven mechanism. Specifically, a \mathbb{Z}_2 Berry phase will emerge at large U due to the Hilbert space restriction (Mottness), which strongly suppresses the mobility of single particle propagation as compared to $U = 0$. However, the kinetic energy of the electrons (holes) can be greatly restored by forming an interlayer spin-singlet pairing, which naturally results in a superconducting state even for relatively small J_{\perp} . An effective hard-core bosonic model is further proposed to estimate the superconducting transition temperature at the mean-field level.

Introduction.—Ever since the revelation of high-temperature superconductivity (SC) in cuprates [1–3] – commonly recognized as a doped Mott insulator – the quest to understand the relationship between the pairing mechanism of unconventional SC and strong electron correlations has persisted as an enduring challenge [3, 4]. The recent experimental breakthrough [5–8], revealing high-temperature superconductivity in pressurized single crystals of $\text{La}_3\text{Ni}_2\text{O}_7$ (LNO), has aroused broad interest. With an observed maximum SC transition temperature T_c reaching 80K under pressures exceeding 14GPa [5], LNO presents a new platform to delve into and scrutinize unconventional pairing mechanisms.

LNO features a layered structure wherein each unit cell incorporates two conductive NiO_2 layers, paralleling the CuO_2 layer found in cuprates. Insights drawn from density functional theory (DFT) [5, 9–15] calculation suggest that the low-energy behaviors in LNO are dominated by two e_g orbitals of Ni, namely $3d_{x^2-y^2}$ and $3d_{z^2}$ with the filling $\nu \approx 1/4$ and $\nu \approx 1/2$, respectively, which has been further verified by Hall coefficient transport measurements [16–18], as well as the volume counting of the Fermi surface observed in Angle-resolved photoemission spectroscopy (ARPES) [19, 20]. When under pressure, the interlayer Ni-O-Ni bonding angle changes from 168° to a straightened 180° , which significantly enhances the interlayer coupling. Furthermore, the pronounced Coulomb repulsion within the Ni-3d orbitals merits attention, aligning with the latest experimental data that posits LNO as nearing a Mott phase and exhibiting non-Fermi-liquid traits above T_c , marked by a linearly temperature-dependent resistivity that extends up to 300K [5, 6, 8].

Two prevalent theoretical starting points exist for describing the SC pairing mechanism in LNO. One relies on a weak coupling approach [10, 21–25], attribut-

ing the SC pairing to the instability of Fermi pockets with spin fluctuations as the pairing glue. Alternatively, the strong-coupling perspective [10, 21, 22, 25–33] emphasizes the role of interlayer exchange between the d_{z^2} orbitals within a unit cell. Regardless of the approach taken, many works point out that it is the spin exchange interaction, which is the residual effect of Coulomb repulsion (on-site Hubbard repulsion), rather than the Coulomb repulsion itself, to be considered as the key driver in the pairing mechanism. This focus may arise from a clear difference between LNO and cuprates: the doped hole density in the $d_{x^2-y^2}$ orbital for LNO ($\delta = 2(1 - \nu) \approx 0.5$), is significantly larger than that in cuprates. In cuprate systems [1, 2], such high doping levels correspond to the “Fermi-liquid” phase, seen as the breakdown of the “Mottness”. As a result, one might initially consider the Coulomb repulsion in the $d_{x^2-y^2}$ orbital of LNO to be irrelevant. If that is the case, such high T_c as observed in experimental data would necessitate a relatively dominant spin-exchange interaction to facilitate the formation of robust Copper pairs.

However, as we will show, the density matrix renormalization group (DMRG) results indicate that the on-site Hubbard interaction indeed substantially enhances the pairing strength, particularly when the intermediate interlayer spin exchange coupling is close to estimation from DFT calculations [5, 9–12, 15]. This numerical evidence offers a compelling hint that the Coulomb interaction itself still plays a significant role in the pairing mechanism. Based on this, we will further demonstrate that the motion of a single hole is severely restricted due to the accumulation of an emergent \mathbb{Z}_2 Berry phase, which arises from the restricted Hilbert space due to the strong on-site Hubbard interaction. Only the channel of inter-layer hole pairs on the background of inter-layer singlet spin pairs remains unvanishing weight because the

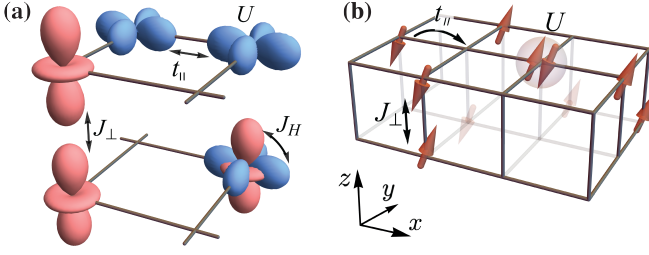


FIG. 1. (a) Schematic representation of the low-lying two-orbital physics in LNO: the red d_{z^2} orbital displays interlayer spin exchange coupling J_\perp , while the blue $d_{x^2-y^2}$ orbital features intralayer hopping term t_\parallel as well as on-site Hubbard interaction U . The Hund's coupling J_H links these two orbitals. (b) Minimal model for d_{z^2} orbital, applicable when J_H is strong enough to align the spins between the $d_{x^2-y^2}$ and d_{z^2} orbitals.

\mathbb{Z}_2 Berry phase can be fully canceled [shown in Fig. 3(b)]. This kinetic-energy-driven pairing mechanism originates directly from the strong Coulomb repulsion, which is applicable across a wide range of hole doping concentrations and is not sensitive to other orbital specifics, such as particular inter-orbital couplings.

Binding energy from Hubbard repulsion.—We first analyze LNO and establish our minimal model. The electronic correlation in the nearly half-filled d_{z^2} orbitals is remarkably strong, as supported by experiments showing that the bands mainly contributed by d_{z^2} orbitals lie below the Fermi surface, are much flatter, and exhibit strong band renormalization (5-8 times) compared with the bands contributed by $d_{x^2-y^2}$ orbitals [19, 34]. Additionally, numerical calculations including DMRG [35] and dynamical mean-field theory (DMFT) [36] that consider multiple orbitals demonstrate that charge carriers are primarily contributed by $d_{x^2-y^2}$ orbitals, rather than d_{z^2} orbitals, and that inter-orbital Hund's coupling plays an important role in the formation of superconductivity.

Therefore, it is reasonable to consider a scenario in which the majority of electrons in the nearly half-filled d_{z^2} orbitals tend to localize, forming local magnetic moments, while their charge degrees of freedom become nearly frozen. This phenomenon can be attributed to the emergence of an orbital-selective Mott transition, predominantly driven by Hund's coupling among the distinct d -orbitals [37–39]. Consequently, as shown in Fig. 1(a), the only relevant interactions are the interlayer spin exchange interaction J_\perp in d_{z^2} orbitals, the intralayer hopping t_\parallel and on-site Coulomb interaction U in $d_{x^2-y^2}$ orbitals (the $d_{x^2-y^2}$ orbital exhibits negligible interlayer single-particle tunneling), as well as the Hund's coupling J_H between different orbitals. Here U and J_\perp are treated as independent parameters to investigate the effect of Mottness. Other allowed complicated interactions in generic multi-orbital systems [39], such as interorbital hopping, are renormalized to be very small due to strong

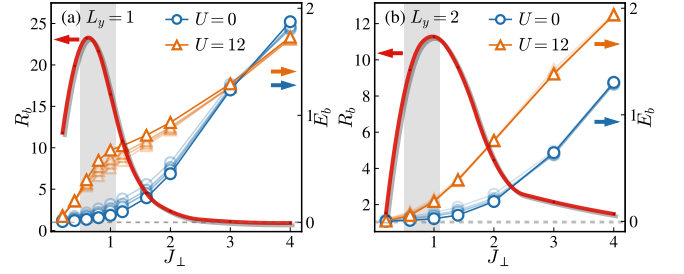


FIG. 2. The binding energy E_b for different on-site repulsion U and the corresponding ratio R_b as a function of interlayer coupling J_\perp with $L_y = 1, 2$ for panel (a) and (b), respectively. The system length is $L_x = 8, 12, 16, 32$ for markers of decreasing transparency. The hole doping is fixed at $\delta = 1/2$. The horizontal dashed lines mark $R_b = 1$ and $E_b = 0$. The shaded areas indicate the experimental relevant regions of J_\perp .

correlation effects [40]. The inter-orbital Coulomb interaction effectively only provides a chemical potential shift to the $d_{x^2-y^2}$ orbitals due to the nearly fixed particle number of d_{z^2} orbitals.

Notably, the strong J_H tends to polarize the spin in different orbitals so that in the large J_H limit, the interlayer exchange interaction J_\perp for d_{z^2} orbital can transfer to $d_{x^2-y^2}$ orbital [27] after integrating out the d_{z^2} local moments. Therefore, we propose the single-band minimal model describing the $d_{x^2-y^2}$ orbital with filling $\nu \approx 1/4$, as specified in [cf. Fig. 1(b)]:

$$H_{t_\parallel-U-J_\perp} = -t_\parallel \sum_{\langle ij \rangle \alpha \sigma} (c_{i\alpha\sigma}^\dagger c_{j\alpha\sigma} + \text{h.c.}) - \mu \sum_{i\alpha\sigma} n_{i\alpha\sigma} + U \sum_{i\alpha} n_{i\alpha\uparrow} n_{i\alpha\downarrow} + J_\perp \sum_i \mathbf{S}_{i1} \cdot \mathbf{S}_{i2}, \quad (1)$$

where $\sigma = \uparrow, \downarrow$ is the spin orientation, and $\alpha = 1, 2$ denotes the layer index. $\mathbf{S}_{i\alpha}$ and $n_{i\alpha\sigma} = c_{i\alpha\sigma}^\dagger c_{i\alpha\sigma}$ are the local spin operator and electron number operator, respectively. We set the intralayer hopping $t_\parallel = 1$ as the energy unit. The interlayer spin coupling J_\perp and the Hubbard repulsion U are varied independently to investigate the effect of Mottness.

We perform DMRG calculations on a bilayer lattice of size $L_x \times L_y$ with L_y being the shorter side. The total number of sites is $N = L_x \times L_y \times L_z$ with $L_z = 2$. We keep the bond dimension up to 5000 with a typical truncation error $\epsilon \lesssim 10^{-7}$. The binding energy of holes is defined as

$$E_b = 2E(N_h + 1) - E(N_h + 2) - E(N_h), \quad (2)$$

where $E(N_h)$ denotes the ground state energy with the fixed number of doped holes $N_h = N\delta$. The total spin S^z is fixed at 0 and $1/2$ for even and odd numbers of holes respectively. Note that the binding energy has an overall linear dependence of J_\perp since the Hamiltonian scales with J_\perp . Hence, we define a dimensionless ratio

$$R_b = \frac{E_b(U = 12)}{E_b(U = 0)}, \quad (3)$$

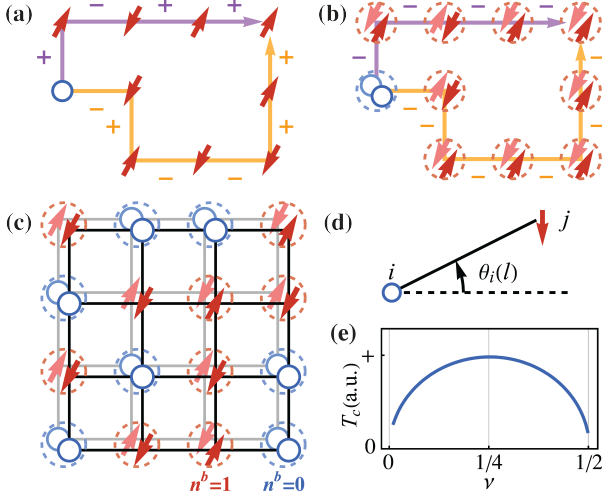


FIG. 3. Schematics of the \mathbb{Z}_2 Berry phase experienced by (a) one hole and (b) hole pairs in the spin-singlet background. Dark (light) blue circles indicate holes in the 1st (2nd) layer, while dark (light) red arrows represent spins in the 1st (2nd) layer. (c) Schematic of the effective hard-core bosonic model in Eq. (8): Spin-singlet pairs correspond to $n_i^b = 1$ and hole pairs correspond to $n_i^b = 0$. (d) Graphic representation of $e^{i\phi}$ in Eq. (7) in the two-dimensional case. (e) Superconducting T_c vs filling ν obtained by the effective model Eq. (8) at the mean-field level, with $J_\perp = 0.6t_\parallel$ and $J_\parallel = 2J_\perp/3$.

to reflect the enhancement of binding energy caused by the Hubbard repulsion. The value of R_b for different J_\perp is depicted by the red lines in Fig. 2, which shows a significant enhancement in binding energy due to on-site repulsion U in both cases of $L_y = 1$ and $L_y = 2$. Notably, this effect is most pronounced when the interlayer coupling J_\perp is relatively small, specifically when $J_\perp \lesssim t_\parallel$, which is in line with the realistic values obtained through DFT calculations. Certainly, such a huge amplification of binding energy still necessitates the assistance of a finite interlayer coupling, albeit not excessively so. This is because at doping $\delta = 1/2$, neither the Hubbard chain nor the two-leg Hubbard ladder is a quasi-one-dimensional superconducting state (as the Luther-Emery liquid), which is consistent with the vanishing binding energy at $J_\perp \rightarrow 0$ shown in Fig. 2. One is referred to Supplemental Material [41] for more numerical evidence. These results suggest that when contemplating pairing mechanisms, strong Coulomb repulsion itself should be regarded as a non-negligible factor rather than simply a contributor to the spin-exchange interaction.

Emergent \mathbb{Z}_2 Berry phases.—In the following, we consider the $U \gg t_\parallel$ regime, in which the doubly occupied states are energetically unfavorable and can be effectively projected out. This results in the t_\parallel - J_\parallel - J_\perp model [26–

28, 42–44]

$$H_{t_\parallel-J_\parallel-J_\perp} = -t_\parallel \sum_{\langle ij \rangle \alpha \sigma} \hat{\mathcal{P}} \left(c_{i\alpha\sigma}^\dagger c_{j\alpha\sigma} + \text{h.c.} \right) \hat{\mathcal{P}} - \mu \sum_{i\alpha\sigma} n_{i\alpha\sigma} + J_\parallel \sum_{\langle ij \rangle \alpha} \mathbf{S}_{i\alpha} \cdot \mathbf{S}_{j\alpha} + J_\perp \sum_i \mathbf{S}_{i1} \cdot \mathbf{S}_{i2}, \quad (4)$$

where J_\parallel denotes the intralayer spin exchange coupling. Based on DFT calculations [5, 9–12], we find $J_\perp \approx 0.6t_\parallel$, $J_\parallel \approx 2J_\perp/3$, and the filling is $\nu \approx 1/4$. The projector $\hat{\mathcal{P}}$ denotes the no-double-occupancy constraint $\sum_\sigma n_{i\alpha\sigma} \leq 1$. This constraint, originating from the strong Hubbard repulsion, introduces a non-trivial sign structure τ_C in the partition function

$$Z_{t_\parallel-J_\parallel-J_\perp} \equiv \text{Tr} e^{-\beta H_{t_\parallel-J_\parallel-J_\perp}} = \sum_C \tau_C W_{t_\parallel-J_\parallel-J_\perp}[C], \quad (5)$$

where β is the inverse temperature, and $W_{t_\parallel-J_\parallel-J_\perp}[C] \geq 0$ denotes the non-negative weight corresponding to each closed loop C of hole-spin configuration evolution. The sign factor τ_C is rigorously defined as follows [41]:

$$\tau_C \equiv (-1)^{N_{\text{ex}}^h} \times (-1)^{N_\downarrow^h}, \quad (6)$$

in which N_{ex}^h represents the total number of exchanges between identical holes, like the fermionic sign structure found in doped semiconductors. The term $(-1)^{N_\downarrow^h}$ in Eq. (6) is identified as the phase-string [45–47], in which N_\downarrow^h accounts for the total number of mutual exchanges between holes and \downarrow -spins. In other words, as illustrated in Fig. 3(a), the hole hopping can accumulate a \mathbb{Z}_2 Berry phase with the sign determined by the orientation of the spin that is exchanged—positive for spin-up and negative for spin-down. It is crucial to emphasize that this emergent sign structure is an exclusive consequence of strong Hubbard repulsion and does not rely on specific model details. This finding is broadly applicable to other strongly correlated systems such as the single-layer t - J model [47, 48] and the Hubbard model [49].

Therefore, the mobility of a single hole is significantly suppressed due to destructive interference effects among various paths, as shown in Fig. 3(a). This theoretical insight is corroborated by DMRG results, which show a rapid decay in the single-particle Green's function $G_{\alpha\sigma}(r) = \langle c_{i,\alpha\sigma}^\dagger c_{j+r,\alpha\sigma} \rangle$ in the presence of a strong Hubbard repulsion, as shown in Fig. 4(a) [41]. On the other hand, this \mathbb{Z}_2 frustration can be fully canceled when two holes from distinct layers pair and move together on the background of spin-singlet interlayer pairs, as depicted in Fig. 3(b). In such configurations, each exchange involving the two-hole composite and spin-singlet will consistently contribute a negative sign, which ultimately cancels out upon completing a closed loop on a bipartite lattice. This phenomenon promotes pairing between interlayer charge (and spin) degrees of freedom, steering the system towards a SC state.

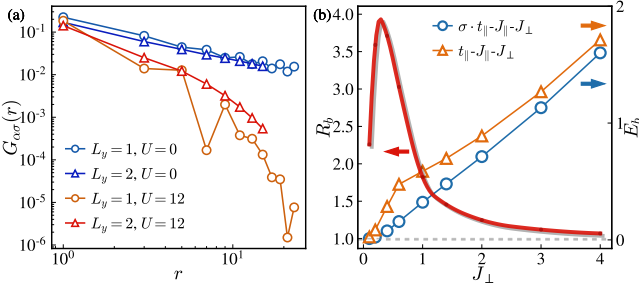


FIG. 4. (a) The single-particle Green's function $G_{\alpha\sigma}(r)$ for different on-site repulsion U with $J_\perp/t_\parallel = 0.6$ for $L_y = 1$ and $J_\perp/t_\parallel = 1.4$ for $L_y = 2$. (b) The binding energy E_b for the $t_\parallel - J_\parallel - J_\perp$ model and $\sigma \cdot t_\parallel - J_\parallel - J_\perp$ model and the corresponding ratio R_b as a function of inter-layer coupling J_\perp with $J_\parallel/t_\parallel = 1/3$ and system length $L_x = 32$. The hole doping is fixed at $\delta = 1/2$. The horizontal dashed lines mark $R_b = 1$ and $E_b = 0$.

To elucidate the physical implication of this unique correlation between holes and spins more explicitly, as mediated by the emergent \mathbb{Z}_2 Berry phase, we employ a unitary transformation [50, 51]

$$e^{i\hat{\Theta}} \equiv \exp \left(-i \sum_{i\alpha} n_{i\alpha}^h \hat{\Omega}_{i\alpha} \right), \quad (7)$$

on the $t_\parallel - J_\parallel - J_\perp$ model in Eq. (4). Here, $n_{i\alpha}^h = 1 - \sum_\sigma c_{i\alpha\sigma}^\dagger c_{i\alpha\sigma}$ denotes the hole number at the site i of layer α . $\hat{\Omega}_{i\alpha}$ accounts for the statistical phase between the hole $n_{i\alpha}^h$ and surrounding spins within the same layer α .

For simplicity, we first focus on the one-dimensional limit with $L_y = 1$ and define $\hat{\Omega}_{i\alpha}^{1D} = \pi \sum_{l>i} n_{l\alpha}^\downarrow$ to compensate the mutual statistics between holes and spins. Thus, the original Hamiltonian is transformed into $e^{-i\hat{\Theta}} H_{t_\parallel - J_\parallel - J_\perp} e^{i\hat{\Theta}} = H_{\sigma t_\parallel - J_\parallel - J_\perp} + H_{\text{string}}$. Here $H_{\sigma t_\parallel - J_\parallel - J_\perp}$ is defined through an additional spin-dependent sign $\sigma = \pm 1$ for $\{\uparrow, \downarrow\}$ on top of the original hopping term, i.e., $-t_\parallel c_{i\alpha\sigma}^\dagger c_{j\alpha\sigma} \rightarrow -\sigma t_\parallel c_{i\alpha\sigma}^\dagger c_{j\alpha\sigma}$, which explicitly removes the sign frustration [41]. However, the cost needed to pay is the additional term $H_{\text{string}} = -J_\perp/2 \sum_i (S_{i1}^+ S_{i2}^- + S_{i1}^- S_{i2}^+) (1 - \Lambda_i^h)$, with $\Lambda_i^h \equiv \exp[i\pi \sum_{l<i} (n_{l1}^h - n_{l2}^h)]$ characterizing the non-local phase shift effects arising from spatially separated holes on distinct chains [41]. Since the interlayer coupling J_\perp implies $\langle S_{i1}^+ S_{i2}^- + S_{i1}^- S_{i2}^+ \rangle < 0$ (denoted by $-g_0$), one can expect that two holes at the distinct chain with the coordinate $r_{\alpha=1}$ and $r'_{\alpha=2}$ will generally acquire a linear pairing potential $V_{\text{string}} \sim J_\perp g_0 |r_{\alpha=1} - r'_{\alpha=2}|$. Such a pairing potential can be validated by comparing the binding energy in the $t_\parallel - J_\parallel - J_\perp$ and $\sigma t_\parallel - J_\parallel - J_\perp$ models through DMRG results shown in Fig. 4(b), which directly demonstrate stronger binding in the $t_\parallel - J_\parallel - J_\perp$ model, particularly around the experimental relevant regime where $J_\perp/t_\parallel \sim 0.6$ [5, 9–12].

Furthermore, the above derivation can be extended to the two-dimension with $L_y \rightarrow \infty$ by setting $\hat{\Omega}_{i\alpha}^{2D} = \sum_{l \neq i} \theta_i(l) n_{l\alpha}^\downarrow$, where $\theta_i(l) \equiv \pm \text{Im} \ln(z_i - z_l)$ with z_i being the complex coordinate of site i , as depicted in Fig. 3(d). Similarly, the interlayer transverse coupling can also induce a strong pairing potential $V_{\text{string}} \sim J_\perp g_0 |r_{\alpha=1} - r'_{\alpha=2}|^2$ between two holes at distinct layers [41]. This additional pairing mechanism is distinguished from traditional spin-exchange pairing by its string-like long-range interaction, which means that it does not necessarily require a very strong J_\perp to bind holes. Furthermore, while the hopping term in two dimensions under the unitary transformation Eq. (7) includes additional, more complex terms compared to the one-dimensional case, these complexities do not substantially affect our preceding arguments.

Effective model.—Based on these physical implications, holes across distinct layers are inclined to form tightly bound $2e$ -charge bosons (blue dashed circles in Fig. 3(c)), and spins tend to form singlet pairs across the two layers, resulting in neutral bosons with $S = 0$ (red dashed circles in Fig. 3(c)). Thus, one can regard an interlayer singlet pair as a hardcore boson $b_i = \frac{1}{\sqrt{2}}(c_{i1\uparrow} c_{i2\downarrow} - c_{i1\downarrow} c_{i2\uparrow})$ with the local particle number $\hat{n}_i^b = b_i^\dagger b_i \leq 1$. Then, with the standard Brillouin-Wigner perturbation theory [41], the Hamiltonian in Eq. (4) can be reduced to an effective Hamiltonian in the low-energy subspace $\mathcal{H} = \bigotimes_i \text{span}\{|0\rangle, b_i^\dagger|0\rangle\}$, i.e.,

$$H_{\text{eff}} = -w \sum_{\langle ij \rangle} (b_i^\dagger b_j + \text{h.c.}) - V \sum_{\langle ij \rangle} \hat{n}_i^b \hat{n}_j^b - \lambda \sum_i \hat{n}_i^b \quad (8)$$

where $w = 8t_\parallel^2/3J_\perp$ denotes the effective hopping, $V = J_\parallel^2/8J_\perp$ denotes a weak neighboring attraction with $V \ll w$ since $t_\parallel \gg J_\parallel$, and $\lambda = 3J_\perp/4 + 2\mu$ is the chemical potential associated with the filling ν .

The effective model H_{eff} in Eq. (8) describes a single-layer hard-core Bose system with a weak nearest-neighbor attractive interaction, as shown in Fig. 3(c). In the one-dimensional scenario, H_{eff} simplifies to a single chain and can be analytically solved using the bosonization method after applying the Jordan-Wigner transformation [41]. This results in a Luther-Emery liquid, characterized by an SC exponent $K_{\text{SC}} < 1$. In the two-dimensional scenario, one can perform a self-consistent mean-field calculation with the order parameter $\langle b_i \rangle = \sqrt{\rho_s}$ [41]. Our findings indicate that the b -bosons will enter a superfluid phase with $\rho_s \neq 0$ at zero temperature unless 2ν is an integer. This phase corresponds to the SC phase in the original fermionic system, marked by the condensation of Cooper pairs. At finite temperatures, the coherence of singlet pairs would be disrupted by the thermal fluctuation and then undergo a Kosterlitz-Thouless (KT) transition at the critical temperature T_c . As a result, the SC phase transition temperature can be

estimated by the KT temperature [52] $T_c = \frac{8\pi t_{\parallel}^2}{3J_{\perp}}\rho_s$, of which the filling dependence is shown in Fig. 3(e). Our results indicate that T_c peaks at $\nu = 1/4$, aligning with the actual situation of the $d_{x^2-y^2}$ orbitals in LNO. In contrast, T_c is drastically suppressed at $\nu = 1/2$, associated with the undoped featureless Mott insulator, also known as a symmetric mass generation (SMG) insulator [53–57].

Discussion.—In this work, the pairing mechanism in the high- T_c SC material $\text{La}_3\text{Ni}_2\text{O}_7$ has been explored, in which a significant role of the Coulomb repulsion U among d -orbital electrons has been revealed. Although a non-zero interlayer superexchange coupling J_{\perp} is essential for the pairing, the binding energy is found to be strongly enhanced with U tuned into the Mott regime as opposed to $U = 0$. In the former regime (large U), the propagation of the single electron (hole) becomes severely frustrated due to the accumulation of a \mathbb{Z}_2 Berry phase (phase-string). Such frustration can be completely canceled out when two holes are paired up with the help of J_{\perp} such that the strong suppression of the kinetic energy can be effectively released. The recent development of flat-band superconductors can be regarded as a single-particle version of this picture. In that case, the kinetic energy is quenched due to the lattice interference pattern, but it can be restored after forming Cooper pairs [58–60]. By contrast, by turning off this Berry phase artificially, the binding is also suppressed even in the large U case. It means that the pairing in the Mott regime is indeed substantially driven up by saving the kinetic energy [61, 62], with the magnitude of about 10-20 times larger than that in the $U = 0$ case around $J_{\perp}/t_{\parallel} \sim 1$. The latter regime (small U) has been studied in other approaches [25]. Note that though the latter mechanism may also yield a similar effective Hamiltonian as in Eq. (8) in the BEC limit [25], it generally requires a much larger J_{\perp} exceeding the hopping integral t_{\parallel} .

Moreover, at the high-temperature phase, the spin-singlet pairs are destroyed, and hence the strong \mathbb{Z}_2 Berry phase frustration that can be experienced by both single hole and hole pairs, resulting in a loss of coherence of the charge degrees of freedom. The scattering between holes and random phase (flux) can naturally give rise to a linear- T dependence of the electric resistivity [63, 64], which is consistent with the experimental measurement in LNO [5, 6, 8].

Acknowledgments.—We acknowledge stimulating discussions with Fan Yang, Guang-Ming Zhang, Shuai Chen, Ji-Si Xu, and Zhao-Yi Zeng. We are especially grateful to Fan Yang for his valuable suggestions on material modeling. J.-X.Z., H.-K.Z., Z.-Y.W. are supported by MOST of China (Grant No. 2021YFA1402101) and NSF of China (Grant No. 12347107); Y.-Z.Y. is supported by the National Science Foundation Grant No. DMR-2238360.

* These two authors contributed equally to this work; zhangjx.phy@gmail.com

† These two authors contributed equally to this work; zhk20@mails.tsinghua.edu.cn

- [1] E. Fradkin, S. A. Kivelson, and J. M. Tranquada, Colloquium: Theory of intertwined orders in high temperature superconductors, *Rev. Mod. Phys.* **87**, 457 (2015).
- [2] B. Keimer, S. A. Kivelson, M. R. Norman, S. Uchida, and J. Zaanen, From quantum matter to high-temperature superconductivity in copper oxides, *Nature* **518**, 179 (2015).
- [3] P. A. Lee, N. Nagaosa, and X.-G. Wen, Doping a Mott insulator: Physics of high-temperature superconductivity, *Rev. Mod. Phys.* **78**, 17 (2006).
- [4] D. J. Scalapino, A common thread: The pairing interaction for unconventional superconductors, *Rev. Mod. Phys.* **84**, 1383 (2012).
- [5] H. Sun, M. Huo, X. Hu, J. Li, Z. Liu, Y. Han, L. Tang, Z. Mao, P. Yang, B. Wang, J. Cheng, D.-X. Yao, G.-M. Zhang, and M. Wang, Signatures of superconductivity near 80 K in a nickelate under high pressure, *Nature* **621**, 493 (2023).
- [6] Y. Zhang, D. Su, Y. Huang, H. Sun, M. Huo, Z. Shan, K. Ye, Z. Yang, R. Li, M. Smidman, M. Wang, L. Jiao, and H. Yuan, High-temperature superconductivity with zero-resistance and strange metal behavior in $\text{La}_3\text{Ni}_2\text{O}_7$, arXiv 10.48550/arxiv.2307.14819 (2023).
- [7] J. Hou, P. T. Yang, Z. Y. Liu, J. Y. Li, P. F. Shan, L. Ma, G. Wang, N. N. Wang, H. Z. Guo, J. P. Sun, Y. Uwatoko, M. Wang, G. M. Zhang, B. S. Wang, and J. G. Cheng, Emergence of high-temperature superconducting phase in the pressurized $\text{La}_3\text{Ni}_2\text{O}_7$ crystals, arXiv 10.48550/arxiv.2307.09865 (2023).
- [8] Z. Liu, M. Huo, J. Li, Q. Li, Y. Liu, Y. Dai, X. Zhou, J. Hao, Y. Lu, M. Wang, and H.-H. Wen, Electronic correlations and energy gap in the bilayer nickelate $\text{La}_3\text{Ni}_2\text{O}_7$, arXiv 10.48550/arxiv.2307.02950 (2023).
- [9] D. A. Shilenko and I. V. Leonov, Correlated electronic structure, orbital-selective behavior, and magnetic correlations in double-layer $\text{La}_3\text{Ni}_2\text{O}_7$ under pressure, arXiv 10.48550/arxiv.2306.14841 (2023).
- [10] H. Sakakibara, N. Kitamine, M. Ochi, and K. Kuroki, Possible high T_c superconductivity in $\text{La}_3\text{Ni}_2\text{O}_7$ under high pressure through manifestation of a nearly-half-filled bilayer Hubbard model, arXiv 10.48550/arxiv.2306.06039 (2023).
- [11] V. Christiansson, F. Petocchi, and P. Werner, Correlated electronic structure of $\text{La}_3\text{Ni}_2\text{O}_7$ under pressure, arXiv 10.48550/arxiv.2306.07931 (2023).
- [12] Y. Zhang, L.-F. Lin, A. Moreo, and E. Dagotto, Electronic structure, orbital-selective behavior, and magnetic tendencies in the bilayer nickelate superconductor $\text{La}_3\text{Ni}_2\text{O}_7$ under pressure, arXiv 10.48550/arxiv.2306.03231 (2023).
- [13] Y. Zhang, L.-F. Lin, A. Moreo, T. A. Maier, and E. Dagotto, Structural phase transition, s_{\pm} -wave pairing and magnetic stripe order in the bilayered nickelate superconductor $\text{La}_3\text{Ni}_2\text{O}_7$ under pressure, arXiv e-prints, arXiv:2307.15276 (2023), arXiv:2307.15276.
- [14] Y. Zhang, L.-F. Lin, A. Moreo, T. A. Maier, and E. Dagotto, Trends of electronic structures and s_{\pm} -wave

- pairing for the rare-earth series in bilayer nickelate superconductor $R_3\text{Ni}_2\text{O}_7$, [arXiv e-prints](#), [arXiv:2308.07386](#) (2023), [arXiv:2308.07386](#).
- [15] Y. Wang, K. Jiang, Z. Wang, F.-C. Zhang, and J. Hu, [Electronic structure and superconductivity in bilayer \$\text{La}_3\text{Ni}_2\text{O}_7\$](#) (2024), [arXiv:2401.15097](#).
 - [16] S. Taniguchi, T. Nishikawa, Y. Yasui, Y. Kobayashi, J. Takeda, S.-i. Shamoto, and M. Sato, Transport, magnetic and thermal properties of $\text{La}_3\text{Ni}_2\text{O}_{7-\delta}$, *Journal of the Physical Society of Japan* **64**, 1644 (1995), <https://doi.org/10.1143/JPSJ.64.1644>.
 - [17] Y. Kobayashi, S. Taniguchi, M. Kasai, M. Sato, T. Nishioka, and M. Kontani, Transport and magnetic properties of $\text{La}_3\text{Ni}_2\text{O}_7$ and $\text{La}_4\text{Ni}_3\text{O}_{10-\delta}$, *Journal of the Physical Society of Japan* **65**, 3978 (1996), <https://doi.org/10.1143/JPSJ.65.3978>.
 - [18] M. Wang, H.-H. Wen, T. Wu, D.-X. Yao, and T. Xiang, Normal and superconducting properties of $\text{La}_3\text{Ni}_2\text{O}_7$ (2024), [arXiv:2406.04837](#).
 - [19] J. Yang, H. Sun, X. Hu, Y. Xie, T. Miao, H. Luo, H. Chen, B. Liang, W. Zhu, G. Qu, C.-Q. Chen, M. Huo, Y. Huang, S. Zhang, F. Zhang, F. Yang, Z. Wang, Q. Peng, H. Mao, G. Liu, Z. Xu, T. Qian, D.-X. Yao, M. Wang, L. Zhao, and X. J. Zhou, Orbital-dependent electron correlation in double-layer nickelate $\text{La}_3\text{Ni}_2\text{O}_7$, *Nature Communications* **15**, 4373 (2024).
 - [20] Y. Liu, M. Ou, H. Chu, H. Yang, Q. Li, Y. Zhang, and H.-H. Wen, [Growth and characterization of the \$\text{La}_3\text{Ni}_2\text{O}_{7-\delta}\$ thin films: dominant contribution of the \$d_{x^2-y^2}\$ orbital at ambient pressure](#) (2024), [arXiv:2406.08789](#).
 - [21] Q.-G. Yang, D. Wang, and Q.-H. Wang, Possible s_{\pm} -wave superconductivity in $\text{La}_3\text{Ni}_2\text{O}_7$, [arXiv 10.48550/arxiv.2306.03706](#) (2023).
 - [22] Y. Gu, C. Le, Z. Yang, X. Wu, and J. Hu, Effective model and pairing tendency in bilayer Ni-based superconductor $\text{La}_3\text{Ni}_2\text{O}_7$, [arXiv 10.48550/arxiv.2306.07275](#) (2023).
 - [23] F. Lechermann, J. Gondolf, S. Bötzel, and I. M. Eremin, Electronic correlations and superconducting instability in $\text{La}_3\text{Ni}_2\text{O}_7$ under high pressure, [arXiv 10.48550/arxiv.2306.05121](#) (2023).
 - [24] Y.-B. Liu, J.-W. Mei, F. Ye, W.-Q. Chen, and F. Yang, The s_{\pm} -Wave Pairing and the Destructive Role of Apical-Oxygen Deficiencies in $\text{La}_3\text{Ni}_2\text{O}_7$ Under Pressure, [arXiv 10.48550/arxiv.2307.10144](#) (2023).
 - [25] D.-C. Lu, M. Li, Z.-Y. Zeng, W. Hou, J. Wang, F. Yang, and Y.-Z. You, Superconductivity from Doping Symmetric Mass Generation Insulators: Application to $\text{La}_3\text{Ni}_2\text{O}_7$ under Pressure, [arXiv \(2023\)](#), [2308.11195](#).
 - [26] X.-Z. Qu, D.-W. Qu, J. Chen, C. Wu, F. Yang, W. Li, and G. Su, Bilayer $t-J-J_{\perp}$ model and magnetically mediated pairing in the pressurized nickelate $\text{La}_3\text{Ni}_2\text{O}_7$, *Phys. Rev. Lett.* **132**, 036502 (2024).
 - [27] C. Lu, Z. Pan, F. Yang, and C. Wu, Interlayer-coupling-driven high-temperature superconductivity in $\text{La}_3\text{Ni}_2\text{O}_7$ under pressure, *Phys. Rev. Lett.* **132**, 146002 (2024).
 - [28] H. Oh and Y.-H. Zhang, Type II t - J model and shared antiferromagnetic spin coupling from Hund's rule in superconducting $\text{La}_3\text{Ni}_2\text{O}_7$, [arXiv e-prints](#) (2023), [arXiv:2307.15706](#).
 - [29] K. Jiang, Z. Wang, and F.-C. Zhang, High Temperature Superconductivity in $\text{La}_3\text{Ni}_2\text{O}_7$, [arXiv 10.48550/arxiv.2308.06771](#) (2023).
 - [30] Y.-f. Yang, G.-M. Zhang, and F.-C. Zhang, Minimal effective model and possible high- T_c mechanism for superconductivity of $\text{La}_3\text{Ni}_2\text{O}_7$ under high pressure, [arXiv 10.48550/arxiv.2308.01176](#) (2023).
 - [31] W. Wu, Z. Luo, D.-X. Yao, and M. Wang, Charge Transfer and Zhang-Rice Singlet Bands in the Nickelate Superconductor $\text{La}_3\text{Ni}_2\text{O}_7$ under Pressure, [arXiv 10.48550/arxiv.2307.05662](#) (2023).
 - [32] Y. Shen, M. Qin, and G.-M. Zhang, Effective bilayer model Hamiltonian and density-matrix renormalization group study for the high- T_c superconductivity in $\text{La}_3\text{Ni}_2\text{O}_7$ under high pressure, [arXiv 10.48550/arxiv.2306.07837](#) (2023).
 - [33] Z. Liao, L. Chen, G. Duan, Y. Wang, C. Liu, R. Yu, and Q. Si, Electron correlations and superconductivity in $\text{La}_3\text{Ni}_2\text{O}_7$ under pressure tuning, [arXiv 10.48550/arxiv.2307.16697](#) (2023).
 - [34] Y. Li, X. Du, Y. Cao, C. Pei, M. Zhang, W. Zhao, K. Zhai, R. Xu, Z. Liu, Z. Li, J. Zhao, G. Li, Y. Qi, H. Guo, Y. Chen, and L. Yang, [Electronic correlation and pseudogap-like behavior of high-temperature superconductor \$\text{La}_3\text{Ni}_2\text{O}_7\$](#) (2024), [arXiv:2407.07501](#).
 - [35] X.-Z. Qu, D.-W. Qu, W. Li, and G. Su, [Roles of hund's rule and hybridization in the two-orbital model for high- \$t_c\$ superconductivity in the bilayer nickelate](#) (2023), [arXiv:2311.12769](#).
 - [36] Y.-H. Tian, Y. Chen, J.-M. Wang, R.-Q. He, and Z.-Y. Lu, Correlation effects and concomitant two-orbital s_{\pm} -wave superconductivity in $\text{La}_3\text{Ni}_2\text{O}_7$ under high pressure, *Phys. Rev. B* **109**, 165154 (2024).
 - [37] L. de' Medici, S. R. Hassan, M. Capone, and X. Dai, Orbital-selective mott transition out of band degeneracy lifting, *Phys. Rev. Lett.* **102**, 126401 (2009).
 - [38] L. de' Medici, G. Giovannetti, and M. Capone, Selective mott physics as a key to iron superconductors, *Phys. Rev. Lett.* **112**, 177001 (2014).
 - [39] A. Georges, L. d. Medici, and J. Mravlje, Strong correlations from hund's coupling, *Annual Review of Condensed Matter Physics* **4**, 137 (2013).
 - [40] C. Lu, Z. Pan, F. Yang, and C. Wu, [Interplay of two \$e_g\$ orbitals in superconducting \$\text{La}_3\text{Ni}_2\text{O}_7\$ under pressure](#) (2023), [arXiv:2310.02915](#).
 - [41] See Supplemental Material at [URL] for further theoretical details and additional numerical results, which includes Refs. [65–67].
 - [42] A. Bohrdt, L. Homeier, C. Reinmoser, E. Demler, and F. Grusdt, Exploration of doped quantum magnets with ultracold atoms, *Annals of Physics* **435**, 168651 (2021), [arXiv:2107.08043](#).
 - [43] A. Bohrdt, L. Homeier, I. Bloch, E. Demler, and F. Grusdt, Strong pairing in mixed-dimensional bilayer antiferromagnetic Mott insulators, *Nature Physics* **18**, 651 (2022), [arXiv:2108.04118](#).
 - [44] S. Hirthe, T. Chalopin, D. Bourgund, P. Bojović, A. Bohrdt, E. Demler, F. Grusdt, I. Bloch, and T. A. Hilker, Magnetically mediated hole pairing in fermionic ladders of ultracold atoms, *Nature (London)* **613**, 463 (2023), [arXiv:2203.10027](#).
 - [45] D. N. Sheng, Y. C. Chen, and Z. Y. Weng, Phase String Effect in a Doped Antiferromagnet, *Phys. Rev. Lett.* **77**, 5102 (1996).
 - [46] Z. Y. Weng, D. N. Sheng, Y.-C. Chen, and C. S. Ting, Phase string effect in the t - J model: General theory, *Phys. Rev. B* **55**, 3894 (1997).
 - [47] K. Wu, Z. Y. Weng, and J. Zaanen, Sign structure of the t - J model, *Phys. Rev. B* **77**, 155102 (2008).

- [48] X. Lu, J.-X. Zhang, S.-S. Gong, D. N. Sheng, and Z.-Y. Weng, [Sign structure in the square-lattice \$t\$ - \$t'\$ - \$j\$ model and numerical consequences](#) (2023), [arXiv:2303.13498](#).
- [49] L. Zhang and Z.-Y. Weng, Sign structure, electron fractionalization, and emergent gauge description of the Hubbard model, *Phys. Rev. B* **90**, 165120 (2014).
- [50] Z. Zhu, D. N. Sheng, and Z.-Y. Weng, Pairing versus phase coherence of doped holes in distinct quantum spin backgrounds, *Phys. Rev. B* **97**, 115144 (2018).
- [51] H.-K. Zhang, R.-Y. Sun, and Z.-Y. Weng, Pair density wave characterized by a hidden string order parameter, *Phys. Rev. B* **108**, 115136 (2023).
- [52] J. B. Kogut, An introduction to lattice gauge theory and spin systems, *Rev. Mod. Phys.* **51**, 659 (1979).
- [53] J. Wang and Y.-Z. You, Symmetric Mass Generation, *Symmetry* **14**, 1475 (2022), [arXiv:2204.14271](#).
- [54] W. Hou and Y.-Z. You, Variational monte carlo study of symmetric mass generation in a bilayer honeycomb lattice model, *Phys. Rev. B* **108**, 125130 (2023).
- [55] D.-C. Lu, M. Zeng, J. Wang, and Y.-Z. You, Fermi surface symmetric mass generation, *Phys. Rev. B* **107**, 195133 (2023), [arXiv:2210.16304](#).
- [56] D.-C. Lu, J. Wang, and Y.-Z. You, Definition and Classification of Fermi Surface Anomalies, [arXiv e-prints](#), [arXiv:2302.12731](#) (2023), [arXiv:2302.12731](#).
- [57] D.-C. Lu, M. Zeng, and Y.-Z. You, Green's Function Zeros in Fermi Surface Symmetric Mass Generation, [arXiv e-prints](#), [arXiv:2307.12223](#) (2023), [arXiv:2307.12223](#).
- [58] P. Törmä, S. Peotta, and B. A. Bernevig, Superconductivity, superfluidity and quantum geometry in twisted multilayer systems, *Nature Reviews Physics* **4**, 528 (2022).
- [59] S. Peotta and P. Törmä, Superfluidity in topologically nontrivial flat bands, *Nature Communications* **6** (2015).
- [60] S. A. Chen and K. T. Law, Ginzburg-landau theory of flat-band superconductors with quantum metric, *Phys. Rev. Lett.* **132**, 026002 (2024).
- [61] J.-Y. Zhao, S. A. Chen, H.-K. Zhang, and Z.-Y. Weng, Two-Hole Ground State: Dichotomy in Pairing Symmetry, *Phys. Rev. X* **12**, 011062 (2022).
- [62] S. Chen, Z. Zhu, and Z.-Y. Weng, Two-hole ground state wavefunction: Non-BCS pairing in a t - J two-leg ladder, *Phys. Rev. B* **98**, 245138 (2018).
- [63] Z.-C. Gu and Z.-Y. Weng, Charge dynamics in the phase string model for high- T_c superconductors, *Phys. Rev. B* **76**, 024501 (2007).
- [64] C. Chen, J.-X. Zhang, Z.-J. Song, and Z.-Y. Weng, Non-Ioffe-Larkin composition rule and spinon-dictated electric transport in doped Mott insulators, [arXiv:2406.15553](#) (2024).
- [65] H.-C. Jiang, S. Chen, and Z.-Y. Weng, Critical role of the sign structure in the doped Mott insulator: Luther-Emery versus Fermi-liquid-like state in quasi-one-dimensional ladders, *Physical Review B* **102**, 104512 (2020), [1909.01475](#).
- [66] B.-X. Zheng, C.-M. Chung, P. Corboz, G. Ehlers, M.-P. Qin, R. M. Noack, H. Shi, S. R. White, S. Zhang, and G. K.-L. Chan, Stripe order in the underdoped region of the two-dimensional Hubbard model, *Science* **358**, 1155 (2017), [arXiv:1701.00054](#).
- [67] M. Qin, C.-M. Chung, H. Shi, E. Vitali, C. Hubig, U. Schollwöck, S. R. White, and S. Zhang, Absence of Superconductivity in the Pure Two-Dimensional Hubbard Model, *Physical Review X* **10**, 031016 (2020), [arXiv:1910.08931](#).

Supplementary Material for “Strong Pairing Originated from an Emergent \mathbb{Z}_2 Berry Phase in $\text{La}_3\text{Ni}_2\text{O}_7$ ”

In this supplementary material, we offer additional analytical and numerical results to reinforce the conclusions in the main text. In Section I, we present a rigorous derivation of the sign structure for both the $t_{\parallel}\text{-}J_{\parallel}\text{-}J$ model and the $\sigma t_{\parallel}\text{-}J_{\parallel}\text{-}J$ model. Section II offers a comprehensive derivation of the effective attraction interaction, denoted as V_{string} , for both one-dimensional and two-dimensional scenarios. In Section III, we delve into the derivation of the effective model H_{eff} and subsequently explore its physical implications in both one-dimensional and two-dimensional cases. In Section IV, we show more numerical evidences on the enhancement of pairing strength from the on-site repulsion.

I. THE EXACT SIGN STRUCTURE OF THE $t_{\parallel}\text{-}J_{\parallel}\text{-}J_{\perp}$ HAMILTONIAN

In this section, we provide rigorous proof for the partition function of the $t_{\parallel}\text{-}J_{\parallel}\text{-}J$ model and elaborate on the sign structure. We initiate our discussion with the slave-fermion formalism. In this context, the electron operator is represented as $c_{i\alpha\sigma} = f_{i\alpha}^{\dagger} b_{i\alpha\sigma}$, where $f_{i\alpha}^{\dagger}$ refers to the fermionic holon operator and $b_{i\alpha\sigma}$ to the bosonic spinon operator. These relations are governed by the constraint $f_{i\alpha}^{\dagger} f_{i\alpha} + \sum_{\sigma} b_{i\alpha\sigma}^{\dagger} b_{i\alpha\sigma} = 1$. To shed light on the sign structure inherent in this model, we incorporate the Marshall sign into the S_z -spin representation. This is achieved through the substitution $b_{i\alpha\sigma} \rightarrow (-\sigma)^{i+\alpha} b_{i\alpha\sigma}$, which leads to

$$c_{i\alpha\sigma} = (-\sigma)^{i+\alpha} f_i^{\dagger} b_{i\alpha\sigma}. \quad (\text{S1})$$

Consequently, the $\sigma t_{\parallel}\text{-}J_{\parallel}\text{-}J_{\perp}$ model is transformed as follows:

$$H_{t_{\parallel}\text{-}J_{\parallel}\text{-}J_{\perp}} = -t_{\parallel} \left(P_{o\uparrow}^{\parallel} - P_{o\downarrow}^{\parallel} \right) - \frac{J_{\parallel}}{2} \left(Q^{\parallel} + P_{\uparrow\downarrow}^{\parallel} \right) - \frac{J_{\perp}}{2} \left(Q^{\perp} + P_{\uparrow\downarrow}^{\perp} \right), \quad (\text{S2})$$

where

$$P_{o\uparrow}^{\parallel} = \sum_{\langle ij \rangle \alpha} b_{i\alpha\uparrow}^{\dagger} b_{j\alpha\uparrow} f_j^{\dagger} f_i + \text{h.c.}, \quad P_{o\downarrow}^{\parallel} = \sum_{\langle ij \rangle \alpha} b_{i\alpha\downarrow}^{\dagger} b_{j\alpha\downarrow} f_j^{\dagger} f_i + \text{h.c.}, \quad (\text{S3})$$

$$P_{\uparrow\downarrow}^{\parallel} = \sum_{\langle ij \rangle \alpha} b_{i\alpha\uparrow}^{\dagger} b_{j\alpha\downarrow}^{\dagger} b_{i\alpha\downarrow} b_{j\alpha\uparrow} + \text{h.c.}, \quad P_{\uparrow\downarrow}^{\perp} = \sum_i b_{i1\uparrow}^{\dagger} b_{i2\downarrow}^{\dagger} b_{i1\downarrow} b_{i2\uparrow} + \text{h.c.}, \quad (\text{S4})$$

$$Q^{\parallel} = \sum_{\langle ij \rangle \alpha} (n_{i\uparrow} n_{j\downarrow} + n_{i\downarrow} n_{j\uparrow}), \quad Q^{\perp} = \sum_i (n_{i1\uparrow} n_{i2\downarrow} + n_{i1\downarrow} n_{i2\uparrow}) \quad (\text{S5})$$

The operators $P_{o\sigma}^{\parallel}$, $P_{\uparrow\downarrow}^{\parallel}$, and $P_{\uparrow\downarrow}^{\perp}$ represent the intralayer hole-spin nearest-neighbor (NN) exchange, intralayer NN spin superexchange, and interlayer NN spin superexchange, respectively. The terms Q^{\parallel} and Q^{\perp} correspond to potential interactions between NN spins. By utilizing the high-temperature series expansion, we derive the partition function up to all orders [47]

$$\begin{aligned} Z_{t_{\parallel}\text{-}J_{\parallel}\text{-}J_{\perp}} &= \text{Tr} e^{-\beta H_{t_{\parallel}\text{-}J_{\parallel}\text{-}J_{\perp}}} = \text{Tr} \sum_{n=0}^{\infty} \frac{\beta^n}{n!} (-H_{t_{\parallel}\text{-}J_{\parallel}\text{-}J_{\perp}})^n \\ &= \sum_{n=0}^{\infty} \frac{(J_{\perp}\beta/2)^n}{n!} \text{Tr} \left[\sum \dots \left(\frac{2t_{\parallel}}{J_{\perp}} P_{o\uparrow}^{\parallel} \right) \dots \left(\frac{J_{\parallel}}{J_{\perp}} Q^{\parallel} \right) \dots P_{\uparrow\downarrow}^{\perp} \dots \left(-\frac{2t_{\parallel}}{J_{\perp}} P_{o\downarrow}^{\parallel} \right) \dots \left(\frac{J_{\parallel}}{J_{\perp}} P_{\uparrow\downarrow}^{\parallel} \right) \dots Q^{\perp} \dots \right]_n \\ &= \sum_{n=0}^{\infty} (-1)^{N_{\downarrow}^h} \frac{(J_{\perp}\beta/2)^n}{n!} \text{Tr} \left[\sum \dots \left(\frac{2t_{\parallel}}{J_{\perp}} P_{o\uparrow}^{\parallel} \right) \dots \left(\frac{J_{\parallel}}{J_{\perp}} Q^{\parallel} \right) \dots P_{\uparrow\downarrow}^{\perp} \dots \left(\frac{2t_{\parallel}}{J_{\perp}} P_{o\downarrow}^{\parallel} \right) \dots \left(\frac{J_{\parallel}}{J_{\perp}} P_{\uparrow\downarrow}^{\parallel} \right) \dots Q^{\perp} \dots \right]_n \end{aligned} \quad (\text{S6})$$

with the underlying assumption that the NN hopping integral remains positive, signified by $t_{\parallel} > 0$. The notation $[\sum \dots]_n$ encompasses the summation over all n -block production. Owing to the trace, both starting and ending configurations of holes and spins must coincide, ensuring that all contributions to $Z_{t_{\parallel}\text{-}J_{\parallel}\text{-}J_{\perp}}$ are delineated by closed loops of holes and spins. Within this framework, N_{\downarrow}^h quantifies the exchanges between down-spins and holes. Then, we insert a complete Ising basis with holes, given by $\sum_{\phi \in \{l_h\}} |\phi; \{l_h\}\rangle \langle \phi; \{l_h\}| = 1$, between operators inside the

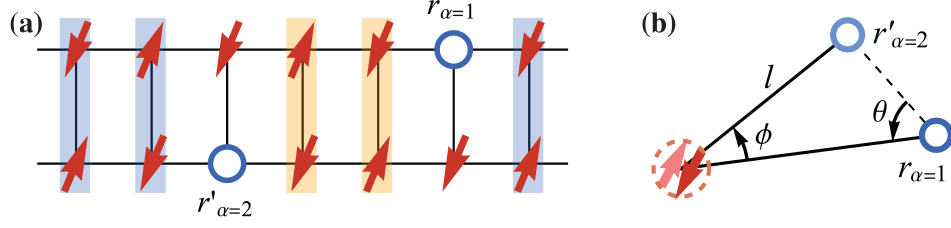


FIG. S1. (a) Illustration of a certain configuration for holes (marked by blue) and spins (marked by red). H_{string} vanishes at the blue rung, while it remains finite at the orange rung. (b) Sketch of positions of holes and spins on a two-layer system, with lighter (darker) color labeling the objects on the first(second) layer.

trace. Here, ϕ specifies the spin configuration, while $\{l_h\}$ indicates the positions of the holes. Therefore, the partition function can be written as a compact expression

$$Z_{t_{\parallel}-J_{\parallel}-J_{\perp}} = \sum_C \tau_C W_{t_{\parallel}-J_{\parallel}-J_{\perp}}[C], \quad (\text{S7})$$

with the relevant sign information is encapsulated by

$$\tau_C^{t_{\parallel}-J_{\parallel}-J_{\perp}} \equiv (-1)^{N_{\text{ex}}^h} \times (-1)^{N_{\downarrow}^h}, \quad (\text{S8})$$

which aligns with the main text. In this context, N_{ex}^h represents the number of hole exchanges arising from the fermionic statistics of the holon f . This sign structure is comprehensively defined across varying doping levels, temperatures, and finite sizes for the $t_{\parallel}-J_{\parallel}-J_{\perp}$ model. Additionally, the non-negative weight $W[C]$ for a closed loop C emerges from a sequence of positive elements within the trace of Eq. (S6).

Furthermore, by introducing the $\sigma t_{\parallel}-J_{\parallel}-J_{\perp}$ model, where the intrinsic spin exchange term remains unchanged, but the hopping term is substituted by

$$H_{\sigma t_{\parallel}} = -t_{\parallel} \sum_{\langle ij \rangle} \sigma c_{i\sigma}^{\dagger} c_{j\sigma} + \text{h.c.}, \quad (\text{S9})$$

in which an additional spin-dependent sign, σ , is integrated into the NN hopping term, cancelling the “-” sign preceding the $P_{o\downarrow}$. As a result, the $\sigma t_{\parallel}-J_{\parallel}-J_{\perp}$ model, under the representation of Eq. (S1), can be rewritten as

$$H_{\sigma t_{\parallel}-J_{\parallel}-J_{\perp}} = -t_{\parallel} (P_{o\uparrow}^{\parallel} + P_{o\downarrow}^{\parallel}) - \frac{J_{\parallel}}{2} (Q^{\parallel} + P_{\uparrow\downarrow}^{\parallel}) - \frac{J_{\perp}}{2} (Q^{\perp} + P_{\uparrow\downarrow}^{\perp}), \quad (\text{S10})$$

with the partition function under the high-temperature series expansion expressed as

$$Z_{\sigma t_{\parallel}-J_{\parallel}-J_{\perp}} = \sum_{n=0}^{\infty} \frac{(J_{\perp}\beta/2)^n}{n!} \text{Tr} \left[\sum \dots \left(\frac{2t_{\parallel}}{J_{\perp}} P_{o\uparrow}^{\parallel} \right) \dots \left(\frac{J_{\parallel}}{J_{\perp}} Q^{\parallel} \right) \dots P_{\uparrow\downarrow}^{\perp} \dots \left(\frac{2t_{\parallel}}{J_{\perp}} P_{o\downarrow}^{\parallel} \right) \dots \left(\frac{J_{\parallel}}{J_{\perp}} P_{\uparrow\downarrow}^{\parallel} \right) \dots Q^{\perp} \dots \right]_n \quad (\text{S11})$$

As the result, the sign structure for $\sigma t_{\parallel}-J_{\parallel}-J_{\perp}$ model is given by

$$\tau_C^{\sigma t_{\parallel}-J_{\parallel}-J_{\perp}} = (-1)^{N_{\text{ex}}^h}, \quad (\text{S12})$$

in which the nontrivial phase string sign $(-1)^{N_{\downarrow}^h}$ vanishes.

In the end, we further clarify the role played by the strong Hubbard repulsion itself in this model. As the hopping integral between the two layers vanishes in the Hamiltonian in Eq. (1) of the main text, projecting our the double occupied states is actually the same as the conventional perturbation process from the single-layer Hubbard model to the t - J model. Note that the J_{\perp} term only involves single occupied states and hence it remains in the same form after the projection. In other words, except for the interlayer superexchange interaction especially in this bilayer lattice, the strong Hubbard repulsion plays the same role as that in the conventional single-layer Mott insulator: opening the Mott gap and hence effectively constraining the Hilbert space by the non-double occupancy projection.

II. EFFECTIVE ATTRACTION INTERACTION V_{string}

In this section, more derivation details about the effective attraction interaction V_{string} in the main text will be discussed for both the one-dimensional and two-dimensional cases.

II.A. One Dimensional Case

In the one-dimensional context, upon employing a unitary transformation $e^{i\hat{\Theta}} \equiv \exp\left(-i \sum_{i\alpha} n_{i\alpha}^h \hat{\Omega}_{i\alpha}\right)$ with $\hat{\Omega}_{i\alpha}^{\text{1D}} = \pi \sum_{l>i} n_{l\alpha}^\downarrow$, the hopping term in $t_{\parallel}\text{-}J_{\parallel}\text{-}J_{\perp}$ model is given by [65]

$$e^{-i\hat{\Theta}} c_{i\alpha\sigma}^\dagger c_{i+1\alpha\sigma} e^{i\hat{\Theta}} = \exp\left[-i \sum_{j,\alpha} n_{j\alpha}^h \pi \sum_{l>j} n_{l\alpha}^\downarrow\right] c_{i\alpha\sigma}^\dagger c_{i+1\alpha\sigma} \exp\left[i \sum_{k,\alpha} n_{k\alpha}^h \pi \sum_{l>k} n_{l\alpha}^\downarrow\right] \quad (\text{S13})$$

$$= \exp\left[-i \sum_{j=i,i+1} \sum_{\alpha} n_{j\alpha}^h \pi \sum_{l>j} n_{l\alpha}^\downarrow\right] c_{i\alpha\sigma}^\dagger c_{i+1\alpha\sigma} \exp\left[i \sum_{k \neq i,i+1} \sum_{\alpha} n_{k\alpha}^h \pi \sum_{l>k} n_{l\alpha}^\downarrow\right] \quad (\text{S14})$$

$$= c_{i\alpha\sigma}^\dagger c_{i+1\alpha\sigma} \exp\left[-i\pi n_{i+1\alpha}^\downarrow\right] \quad (\text{S15})$$

$$= \sigma c_{i\alpha,\sigma}^\dagger c_{i+1\alpha\sigma}. \quad (\text{S16})$$

Similarly, the spin exchange interaction transforms as:

$$e^{-i\hat{\Theta}} S_{i1}^z S_{i2}^z e^{i\hat{\Theta}} = \exp\left[-i \sum_{j,\alpha} n_{j\alpha}^h \pi \sum_{l>j} n_{l,\alpha}^\downarrow\right] c_{i1\uparrow}^\dagger c_{i1\downarrow} c_{i2\downarrow}^\dagger c_{i2\uparrow} \exp\left[i \sum_{k,\alpha} n_{k\alpha}^h \pi \sum_{l>k} n_{l\alpha}^\downarrow\right] = S_{i1}^z S_{i2}^z, \quad (\text{S17})$$

as well as:

$$e^{-i\hat{\Theta}} S_{i1}^+ S_{i2}^- e^{i\hat{\Theta}} = \exp\left[-i \sum_{j,\alpha} n_{j\alpha}^h \pi \sum_{l>j} n_{l\alpha}^\downarrow\right] c_{i1\uparrow}^\dagger c_{i1\downarrow} c_{i2\downarrow}^\dagger c_{i2\uparrow} \exp\left[i \sum_{k,\alpha} n_{k\alpha}^h \pi \sum_{l>k} n_{l\alpha}^\downarrow\right] \quad (\text{S18})$$

$$= \exp\left[-i \sum_{j<i,\alpha} n_{j\alpha}^h \pi \sum_{l>j} n_{l\alpha}^\downarrow\right] c_{i1\uparrow}^\dagger c_{i1\downarrow} c_{i2\downarrow}^\dagger c_{i2\uparrow} \exp\left[i \sum_{k<i,\alpha} n_{k\alpha}^h \pi \sum_{\downarrow>k} n_{l\alpha}^\downarrow\right] \quad (\text{S19})$$

$$= S_{i1}^+ S_{i2}^- \exp\left[i\pi \sum_{l<i} (n_{l1}^h - n_{l2}^h)\right]. \quad (\text{S20})$$

As the result, combining Eq. (S13), Eq. (S17) and Eq. (S18), the total Hamiltonian $t_{\parallel}\text{-}J_{\parallel}\text{-}J_{\perp}$ can be expressed as:

$$e^{-i\hat{\Theta}} H_{t_{\parallel}\text{-}J_{\parallel}\text{-}J_{\perp}} e^{i\hat{\Theta}} = H_{\sigma t_{\parallel}\text{-}J_{\parallel}\text{-}J_{\perp}} + H_{\text{string}}. \quad (\text{S21})$$

Here, $H_{\sigma t_{\parallel}\text{-}J_{\parallel}\text{-}J_{\perp}}$ and H_{string} are defined as:

$$H_{\sigma t_{\parallel}\text{-}J_{\parallel}\text{-}J_{\perp}} = -t_{\parallel} \sum_{\langle ij \rangle \alpha \sigma} \left(\sigma c_{i\alpha\sigma}^\dagger c_{j\alpha\sigma} + \text{h.c.} \right) - \mu \sum_{i\alpha\sigma} n_{i\alpha\sigma} + J_{\parallel} \sum_{\langle ij \rangle \alpha} \mathbf{S}_{i\alpha} \cdot \mathbf{S}_{j\alpha} + J_{\perp} \sum_i \mathbf{S}_{i1} \cdot \mathbf{S}_{i2} \quad (\text{S22})$$

$$H_{\text{string}} = \frac{J_{\perp}}{2} \sum_i (S_{i1}^+ S_{i2}^- + S_{i1}^- S_{i2}^+) (\Lambda_i^h - 1) \quad (\text{S23})$$

with $\Lambda_i^h = \exp\left[i\pi \sum_{l<i} (n_{l1}^h - n_{l2}^h)\right]$. Here, Eq. (S22) is the $\sigma t_{\parallel}\text{-}J_{\parallel}\text{-}J_{\perp}$ model with only the fermionic statistic sign, as depicted in Eq. (S12). Furthermore, given the expectation value of the transverse spin at each rung by $\langle S_{i1}^+ S_{i2}^- + S_{i1}^- S_{i2}^+ \rangle < 0$ (denoted by $-g_0$), it becomes evident that Eq. (S23) vanishes when hole pairs across the rung exist on a background where spins also establish interchain singlet pairing. Nonetheless, when these hole pairs are broken and the two holes are separated by some distance, every rung with spin-singlet pairs located between these

holes will contribute $J_{\perp}g_0/2$ (highlighted by orange shadows in Fig. S1(a)). This results in an energy cost that depends linearly:

$$V_{\text{string}} \sim J_{\perp}g_0 |r_{\alpha=1} - r'_{\alpha=2}|, \quad (\text{S24})$$

where $r_{\alpha=1}$ and $r'_{\alpha=2}$ denote the coordinates of the holes on chain 1 and chain 2, respectively.

II.B. Two Dimensional Case

In the two dimensional case, the unitary transformation can be generalized by setting $\hat{\Omega}_{i\alpha}^{2D} = \sum_{l \neq i} \theta_i(l) n_{l\alpha}^{\downarrow}$. With this transformation, the spin exchange term evolves as:

$$e^{-i\hat{\Theta}} S_{i1}^+ S_{i2}^- e^{i\hat{\Theta}} = S_{i1}^+ S_{i2}^- \exp \left[i \sum_{l \neq i} \theta_i(l) (n_{l1}^h - n_{l2}^h) \right]. \quad (\text{S25})$$

When spin singlets form across the two layers, i.e., $\langle S_{i1}^+ S_{i2}^- \rangle < 0$, the ensuing energy cost from this term can be expressed as:

$$V_{\text{string}} = \left\langle \frac{J_{\perp}}{2} \sum_i e^{-i\hat{\Theta}} (S_{i1}^+ S_{i2}^- + S_{i1}^- S_{i2}^+) e^{i\hat{\Theta}} - \frac{J_{\perp}}{2} \sum_i (S_{i1}^+ S_{i2}^- + S_{i1}^- S_{i2}^+) \right\rangle \quad (\text{S26})$$

$$= -J_{\perp}g_0 \sum_i \cos \left[i \sum_{l \neq i} \theta_i(l) (n_{l1}^h - n_{l2}^h) \right] + \sum_i Jg_0 \quad (\text{S27})$$

$$\approx \frac{J_{\perp}g_0}{2} \int_0^{\infty} r dr \int_0^{2\pi} d\theta \phi^2 + E_{\text{core}} \quad (\text{S28})$$

$$\propto J_{\perp}g_0 \ln R |r_{\alpha=1} - r'_{\alpha=2}|^2 + E_{\text{core}}, \quad (\text{S29})$$

where R is the sample size, and E_{core} represents the ultraviolet energy in proximity to the hole pairs. In the last line of Eq. (S26), the relation $\phi \simeq |r_{\alpha=1} - r'_{\alpha=2}| \sin \theta / l$ is used, and the definition of ϕ , l and θ is illustrated in Fig. S1(b). It is noteworthy that the string tension $\ln R$ in Eq. (S26) approaches infinity as we tend towards the thermodynamic limit. However, the term $g_0 \ln R$ aims to remain finite, thereby avoiding energy divergence.

III. EFFECTIVE MODEL H_{eff}

In this section, more derivation about the hard-core bosonic effective Hamiltonian H_{eff} will be given, and then we will discuss its physical implication using the one-dimensional Abelian bosonization approach and the two-dimensional mean-field theory, respectively.

From our preceding discussions, the local Hilbert space at the i th rung of the original double-layer system can be divided into two subspaces with distinct energy scales:

- low-energy sector \mathcal{V}_0 :

$$|00\rangle_i : E = 0 \quad (\text{S30})$$

$$\frac{1}{\sqrt{2}}(|\uparrow\downarrow\rangle_i - |\downarrow\uparrow\rangle_i) : E = -\frac{3}{4}J_{\perp} \quad (\text{S31})$$

- high-energy sector \mathcal{V}_1 :

$$|\downarrow\downarrow\rangle_i, \quad |\uparrow\uparrow\rangle_i, \quad \frac{1}{\sqrt{2}}(|\uparrow\downarrow\rangle_i + |\downarrow\uparrow\rangle_i) : E = \frac{1}{4}J_{\perp} \quad (\text{S32})$$

$$|\downarrow 0\rangle_i, \quad |\uparrow 0\rangle_i, \quad |0 \downarrow\rangle_i, \quad |0 \uparrow\rangle_i : E = V_{\text{string}} \quad (\text{S33})$$

Then, we can define projective operators P onto the low-energy sector \mathcal{V}_0 as

$$P = \prod_i \sum_{\alpha \in \mathcal{V}_0} |\alpha\rangle\langle\alpha|, \quad (\text{S34})$$

and projective operators Q onto the high-energy sector \mathcal{V}_1 ;

$$Q = 1 - P. \quad (\text{S35})$$

Applying the Brillouin-Wigner perturbation theory, the effective Hamiltonian is given by: $H_{\text{eff}}(E) = PHP - PHQ(QHQ - E)^{-1}QHP$. At the zeroth order, it becomes

$$PH_{\sigma t_{\parallel} - J_{\parallel} - J_{\perp}}P = -\frac{3}{4}J_{\perp} \sum_i n_i^b - 2\mu \sum_i n_i^b, \quad (\text{S36})$$

where $n_i^b = b_i^{\dagger}b_i$ denotes the local number operator for hard-core boson, with the correspondence $b_i = \frac{1}{\sqrt{2}}(c_{i1\uparrow}c_{i2\downarrow} - c_{i1\downarrow}c_{i2\uparrow})$. For the hopping term, the second-order virtual process is expressed as

$$PH_{t_{\parallel}}Q(E - QHQ)^{-1}QH_{t_{\parallel}}P = -\frac{8t_{\parallel}^2}{3J_{\perp} + 4V_{\text{string}}} (b_i^{\dagger}b_j + h.c.). \quad (\text{S37})$$

Similarly, for the intralayer spin exchange interactions, the second-order virtual process is given by

$$PH_{J_{\parallel}}Q(E - QHQ)^{-1}QH_{J_{\parallel}}P = -\frac{J_{\parallel}^2}{8J_{\perp}} n_i^b n_j^b. \quad (\text{S38})$$

As the result, combining Eqs. (S36), (S37) and (S38), the resulting effective Hamiltonian is given by

$$H_{\text{eff}} = \sum_i -w (b_i^{\dagger}b_j + \text{h.c.}) - V \hat{n}_i^b \hat{n}_j^b - \lambda \hat{n}_i^b, \quad (\text{S39})$$

which is consistent with the main text. Here, $w \approx 8t_{\parallel}^2/3J_{\perp}$ denotes effective hopping term for boson, $V = J_{\parallel}^2/8J_{\perp}$ denotes a weak neighbouring attractive interaction and $\lambda = 3J_{\perp}/4 + 2\mu$ is the chemical potential associated with the fillings ν . Note that V_{string} here becomes negligible when the separation distance is very short (only a lattice constant in this case).

III.A. One Dimensional Case: Bosonization

For the one-dimensional scenario, the effective Hamiltonian can be expressed as

$$H[\psi] = -w \sum_i (\psi_i^{\dagger} \psi_{i+1} + \psi_{i+1}^{\dagger} \psi_i) - V \sum_i n_i^b n_{i+1}^b - \lambda \sum_i n_i^b \quad (\text{S40})$$

under the Jordan-Wigner transformation

$$\psi_i = b_i \exp \left(-i\pi \sum_{l>i} n_l \right). \quad (\text{S41})$$

Upon employing standard Abelian bosonization, the relationship between the fermionic and bosonic fields is

$$\psi_i = \frac{\eta}{\sqrt{2\pi a}} e^{ik_b x} e^{-i(\phi_b - \theta_b)} + \frac{\bar{\eta}}{\sqrt{2\pi a}} e^{-ik_b x} e^{-i(-\phi_b - \theta_b)}. \quad (\text{S42})$$

Consequently, the fermionic Hamiltonian, denoted Eq. (S40), transforms to

$$H[\phi, \theta] = \frac{u_b}{2\pi} \int dx \left\{ K_b [\partial_x \theta_b(x)]^2 + \frac{1}{K_b} [\partial_x \phi_b(x)]^2 \right\} - \frac{U}{\pi} \partial_x \phi_b, \quad (\text{S43})$$

which illustrates the low-energy fluctuations of the pairing field, ϕ , with the stiffness constant

$$K_b = 1 + V \frac{2 \sin^2 k_F}{\pi u_b} > 1, \quad (\text{S44})$$

where $k_F = 2\pi\nu$ signifies the effective Fermi momentum. Additionally, the density-density correlation with the hole number operator, denoted by $n_i^h = 1 - \sum_{\alpha\sigma} n_{i\alpha\sigma}/2$, is:

$$\langle n_i^h n_{i+r}^h \rangle = \langle n_i^b n_{i+r}^b \rangle \sim \frac{2}{(2\pi)^2} |r|^{-2K_b} \cos(2k_F r), \quad (\text{S45})$$

where the expression for the density operator is given by $n_x^b = -\frac{1}{\pi} \partial_x \phi_b + \frac{1}{2\pi} [e^{i2k_b x} e^{-2i\phi_b} + \text{h.c.}]$. As a result, from Eq. (S45), we deduce that the charge density exponent is $K_C = 2K_b$. Moreover, the singlet superconducting pairing correlation, $\langle b_i b_{i+r}^\dagger \rangle$ in the fermionic representation is:

$$\langle b_i b_{i+r}^\dagger \rangle = \left\langle \exp \left(-i\pi \sum_{l>i} \hat{n}_l \right) \psi_i \psi_{i+r}^\dagger \exp \left(+i\pi \sum_{l>i+r} \hat{n}_l \right) \right\rangle \sim e^{ik_F r} |r|^{-(1/2)K_b^{-1}}, \quad (\text{S46})$$

so that $K_{SC} = \frac{1}{2} K_b^{-1}$. A key observation is that $K_C K_{SC} = 1$, which characterizes a Luther-Emery liquid. Notably, for $V > 0$ indicating an attractive interaction, $K_b > 1$ from Eq. (S44) implies a heightened SC instability with $K_{SC} < 1$.

III.B. Two Dimensional Case: Mean-Field Theory

In the two-dimensional case, the Hilbert space for distinct sites can be decoupled using the mean field ansatz, $\langle b_i \rangle = \sqrt{\rho_s}$. The resulting mean-field (MF) Hamiltonian becomes:

$$H_{\text{MF}} = \sum_i \left[-s \left(b_i^\dagger + b_i \right) - v n_i^b + \epsilon \right] \quad (\text{S47})$$

with

$$s = \frac{32}{3J_\perp} t_\parallel^2 \sqrt{\rho_s}, \quad v = \frac{J_\parallel^2}{2J_\perp} \rho_s + \frac{3}{4} J_\perp + 2\mu, \quad \epsilon = \frac{32}{3J_\perp} t_\parallel^2 \rho_s + \frac{J_\parallel^2}{4J_\perp} \rho_s^2. \quad (\text{S48})$$

By diagonalizing this two-dimensional on-site Hilbert space, we acquire the local ground state $|\text{GS}\rangle_i$ and its corresponding energy $E_{\text{GS}}(\rho_s)$. Both ρ_s and μ can be determined by minimizing $E_{\text{GS}}(\rho_s)$ with respect to ρ_s , and preserving the filling condition: $\langle \text{GS} | n_i^b | \text{GS} \rangle = 2\nu$.

IV. Additional numerical results and technical details

In the main text, the dimensionless ratio R_b of binding energy is obtained by extrapolation from DMRG results via finite-size scaling with respect to L_x , as shown in Fig. S2. The relation between the dimensionless ratio R_b and system length L_x is obtained by quadratic fitting $f(1/L_x) = c + b/L_x + a/L_x^2$. The curve of the dimensionless ratio vs the interlayer spin-exchange coupling is smoothed by the quadratic spline interpolation.

As J_\perp directly serves as a coefficient in the Hamiltonian, the binding energy E_b naturally scales linearly with J_\perp in general, which makes E_b look relatively small at small J_\perp in FIG. 2 of the main text. Alternatively, we can depict the quantity E_b/J_\perp to see the relative enhancement caused by J_\perp , as shown in FIG. S3. One can see that the difference between $U = 12$ and $U = 0$ becomes larger in E_b/J_\perp compared with FIG. 2 of the main text, especially in the experimental relevant region.

Here we make some clarification about the DMRG results of binding energy shown in the main text. Due to the nature of DMRG, which is believed to provide reliable results only for quasi-1D systems, it is very challenging to generalize the present numerical finding in the enhancement of the binding energy to the 2D limit. This challenge is a common and general issue for the numerical study of 2D strongly correlated systems including the single-layer Hubbard or t - J model [66, 67], not to mention that the bilayer structure here brings extra challenges for increasing the width of the system. However, for the current bilayer model, there is a reason to believe that the numerical

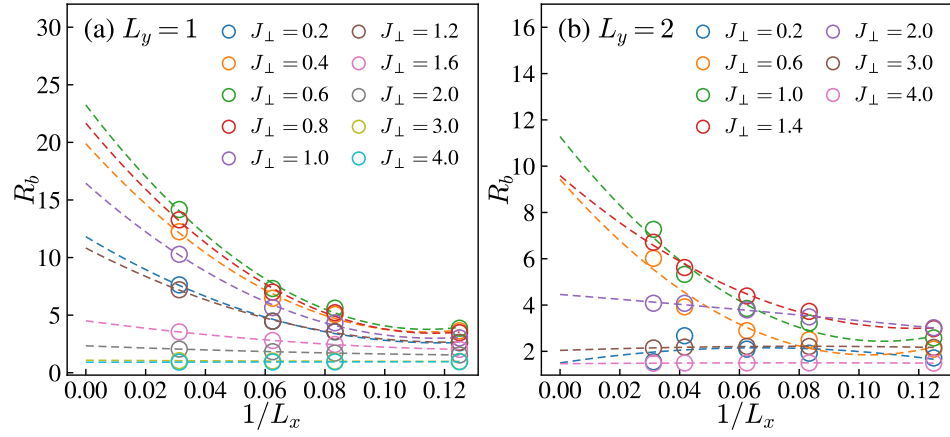


FIG. S2. The extrapolation of the dimensionless ratio R_b vs. system length L_x by quadratic fitting based on data at $L_x = 8, 12, 16, 32$ for $L_y = 1$ in panel (a) and $L_x = 8, 12, 16, 24, 32$ for $L_y = 2$ in panel (b).

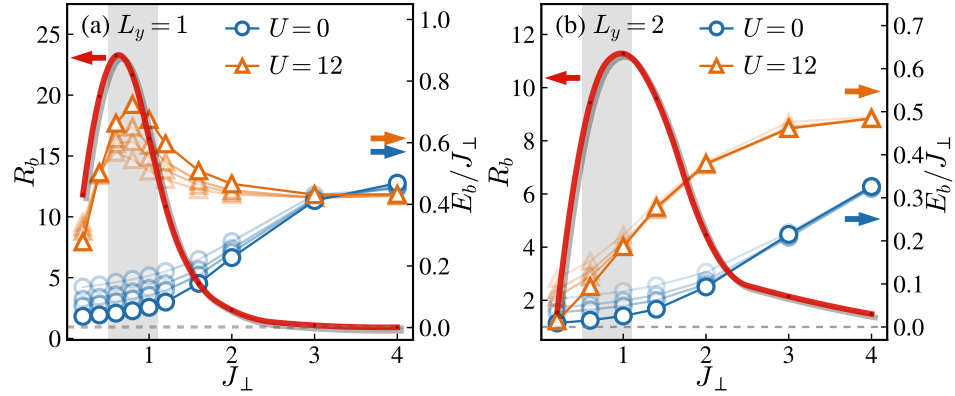


FIG. S3. The binding energy E_b in units of J_\perp for different Hubbard repulsion U and the corresponding ratio R_b as a function of interlayer coupling J_\perp with $L_y = 1, 2$ for panel (a) and (b), respectively. The system length is $L_x = 8, 12, 16, 32$ for markers of decreasing transparency. The hole doping is fixed at $\delta = 1/2$. The shaded areas indicate the experimental relevant regions of J_\perp . The horizontal dashed lines mark $R_b = 1$ and $E_b = 0$.

results of binding energy on narrow systems can indeed be extended to wider 2D systems to a certain extent because the pairing size is quite small (around one or two lattice constants) mainly involving two holes on the two sites of a vertical bond between the two NiO_2 layers [26]. Hence the pairing strength of two holes may be relatively insensitive to the width of each layer as long as the width exceeds the pairing size.

In the main text, we show that the single-particle Green's function $G_{\alpha\sigma}(r)$ in systems with on-site repulsion $U = 12$ decays exponentially for small J_\perp , while that with $U = 0$ decays algebraically. We remark that $G_{\alpha\sigma}(r)$ is symmetric for different layer α and spin σ so only the data for $G_{1\uparrow}(r)$ is depicted. Moreover, we can extract the correlation length ξ_G by fitting $G_{\alpha\sigma}(r) \sim e^{-r/\xi_G}$. Although in certain cases the envelopes of $G_{\alpha\sigma}(r)$ may be closer to shapes of power-law decay, we can still extract the optimal parameter ξ_G from the data of these finite-size systems to see its dependency on J_\perp and U . As shown in Fig. S4, the single-particle correlation length in systems with $U = 12$ is generally shorter than that with $U = 0$. The inverse of the dimensionless ratio $R_G = \xi_G(U = 12)/\xi_G(U = 0)$ is significantly large for $J_\perp \sim t_\parallel$. At $J_\perp \rightarrow 0$, both cases are quasi-long-ranged but as soon as we apply a small J_\perp , systems with $U = 12$ open a single-particle gap while systems with $U = 0$ still keep the single-particle channel gapless until J_\perp is large enough. This further supports the perspective that the on-site repulsion U strongly frustrates the single-particle motion in the presence of a small J_\perp as discussed in the main text.

In the following, we show some other correlators together with their relations with J_\perp and U . The pair-pair correlators for singlets are defined as

$$P_{\alpha\beta}(r) = \langle \Delta_{i,\alpha}^\dagger \Delta_{j,\beta} \rangle, \quad (\text{S49})$$

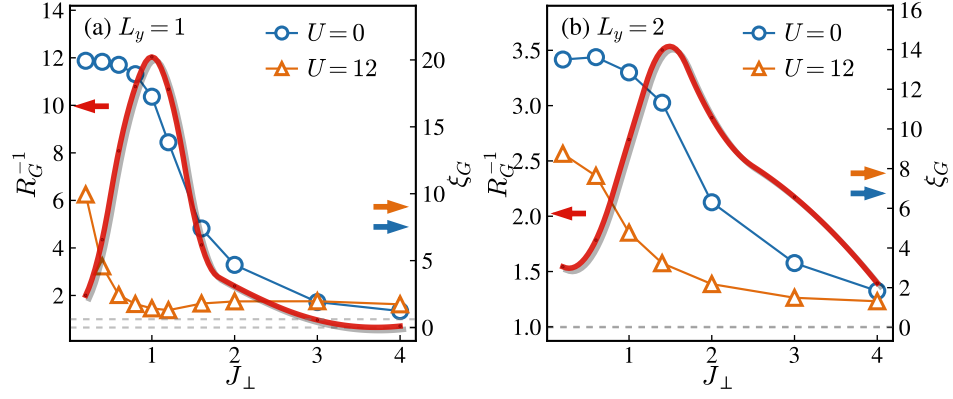


FIG. S4. The correlation length ξ_G extracted from the single-particle Green's function $G_{\alpha\sigma}(r)$ vs. interlayer exchange coupling J_\perp for different on-site repulsion U together with the inverse relative ratio R_G^{-1} . The system size is $64 \times 1 \times 2$ for panel (a) and $32 \times 2 \times 2$ for panel (b), respectively.

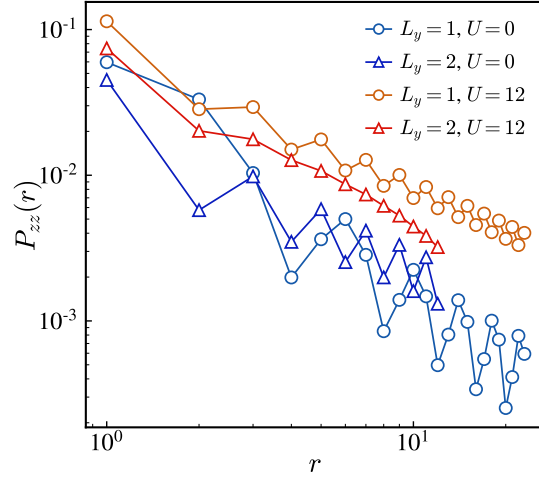


FIG. S5. The pair-pair correlator $P_{zz}(r)$ for different on-site repulsion U with $J_\perp/t_\parallel = 0.6$ for $L_y = 1$ and $J_\perp/t_\parallel = 1.4$ for $L_y = 2$. The system size is $64 \times 1 \times 2$ and $32 \times 2 \times 2$, respectively.

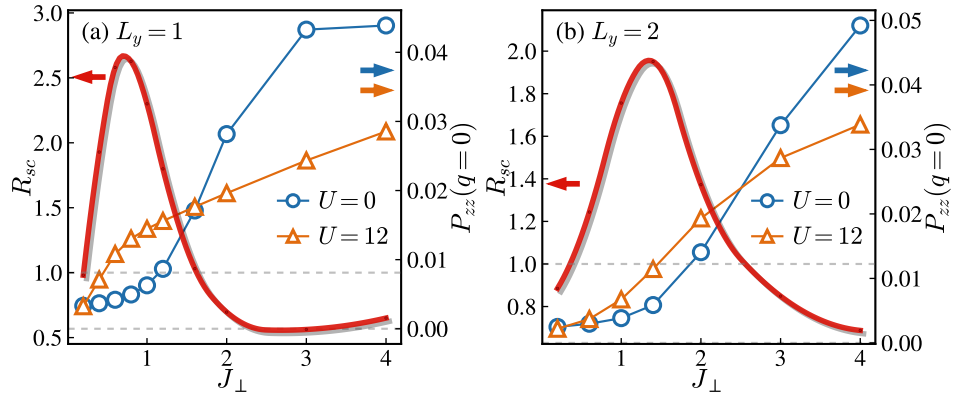


FIG. S6. The overall magnitude $P_{zz}(q=0)$ of the pair-pair correlator $P_{zz}(r)$ vs. interlayer exchange coupling J_\perp for different on-site repulsion U together with the relative ratio R_{sc} . The system size is $64 \times 1 \times 2$ for panel (a) and $32 \times 2 \times 2$ for panel (b), respectively.

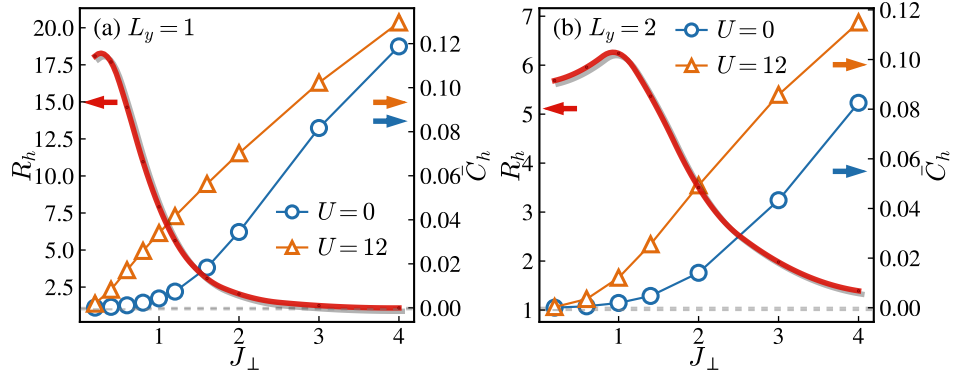


FIG. S7. The averaged interlayer nearest-neighbor holon-holon correlation \bar{C}_h vs. interlayer exchange coupling J_\perp for different on-site repulsion U in systems of (a) $L_y = 1$ and (b) $L_y = 2$. The system length is fixed at $L_x = 32$.

respectively, where $|i - j| = r$ is the real-space distance between lattice site i and j . Here we focus on the correlators along the \hat{x} direction by taking $i = (x, y, \alpha) = (x, 0, 0)$ and $j = (x + r, 0, 0)$ and set the reference site at $x = L_x/4$. $\Delta_{i,\alpha}^\dagger = \frac{1}{\sqrt{2}} \sum_\sigma \sigma c_{i,\sigma}^\dagger c_{i+\alpha,-\sigma}^\dagger$ is the singlet pair creation operator defined at the bond between site i and $i + \alpha$. $\alpha, \beta \in \{\hat{x}, \hat{y}, \hat{z}\}$ denote the bond orientation. The Fourier transform is $P_{\alpha\beta}(q) = |\sum_r P(r) e^{iqr}| / R$, the peak value of which can be regarded as the overall magnitude of the correlation. Fig. S5 shows the typical behavior of the interlayer nearest-neighbor pair-pair correlator $P_{zz}(r)$. One can see that in spite that all of them are quasi-long-ranged, $P_{zz}(r)$ in systems with $U = 12$ is larger than that with $U = 0$ for both $L_y = 1$ and $L_y = 2$. Fig. S6 depicts that the overall magnitude of $P_{zz}(r)$ in systems with $U = 12$ is larger than that with $U = 0$ around $J_\perp \sim t_\parallel$, as indicated by the peak of the dimensionless ratio $R_{sc} = P_{zz}(q = 0, U = 12) / P_{zz}(q = 0, U = 0)$.

We can also investigate the local pairing strength of holes through the holon-holon density correlator between interlayer nearest-neighbor sites

$$C_h(i) = \langle n_{i1}^h n_{i2}^h \rangle - \langle n_{i1}^h \rangle \langle n_{i2}^h \rangle, \quad (\text{S50})$$

where $n_{i\alpha}^h$ is the holon density at site i and layer α defined by $n_{i\alpha}^h = (1 - n_{i\alpha\uparrow})(1 - n_{i\alpha\downarrow})$. We estimate the local pairing strength via the overall magnitude \bar{C}_h by taking average over all sites, i.e., $\bar{C}_h = \sum_i C_h(i) / (L_x L_y)$. As shown in Fig. S7, \bar{C}_h in systems with strong on-site repulsion $U = 12$ is always larger than that with $U = 0$, for both system widths $L_y = 1$ and $L_y = 2$. The relative ratio $R_h = \bar{C}_h(U = 12) / \bar{C}_h(U = 0)$ is also significantly large at $J_\perp \lesssim t_\parallel$. This implies that given a holon at site i and layer 1, it is more likely to find another holon at site i and layer 2 in systems with $U = 12$ than those with $U = 0$. This data provides additional evidence for the enhancement of interlayer pairing strength from the on-site repulsion, compensating for the deficiency that the binding energy shown in the main text mixes the contributions from interlayer and intralayer pairing.